Electronic Supplementary Material (ESI) for Nanoscale.

Experimental and simulation study of self-assembly and adsorption of glycerol monooleate in *n*-dodecane with varying water content onto iron oxide: Electronic supplementary information

Alexander J. Armstrong,[1,2] Rui F. G. Apóstolo,[3,4] Thomas M. McCoy,[2] Finian J. Allen,[1] James Doutch,[1] Beatrice N. Cattoz,[5] Peter J. Dowding,[5] Rebecca J. L. Welbourn,[1] Alexander F. Routh,[2] and Philip J. Camp[4,*]

[1]*ISIS Neutron and Muon Source, Didcot, UK*

[2]*Institute for Energy & Environmental Flows and Department of Chemical Engineering and Biotechnology, University of Cambridge, Cambridge, UK*

[3]*EPCC, Bayes Centre, 47 Potterrow, Edinburgh EH8 9BT, Scotland*

[4]*School of Chemistry, University of Edinburgh, David Brewster Road, Edinburgh EH9 3FJ, Scotland*

[5]*Infineum UK Ltd, Milton Hill, UK*

(Dated: November 25, 2023)

CONTENTS

* Corresponding author: philip.camp@ed.ac.uk

I. MOLECULAR DYNAMICS SIMULATIONS

The Lennard-Jones interaction parameters (diameter σ and well depth ϵ) and partial charges (q) used in the simulations of Fe_2O_3 are shown in Table S1. These parameters were taken from Ref. 1 in the case where $\epsilon_{Fe} = \epsilon_O$. All other parameters were taken from the L-OPLS-AA force field [2–7] as described in the main article, and cross interactions were computed using geometric-mean mixing rules.

TABLE S1. Lennard-Jones parameters σ and ϵ, and partial charges q, for atoms of the Fe_2O_3 surfaces.

Atom	σ / Å	ϵ / kcal mol^{-1}	q / e	Note
Fe	2.20	0.1699	+0.771	Ref. 1 – used in this work
O	2.96	0.1699	−0.514	Ref. 1 – used in this work
Fe	2.09	0.28	+0.645	Ref. 8
O	2.41	0.25	−0.430	Ref. 8

Recent work on refitting the force-field parameters, in conjunction with the L-OPLS-AA force field [2–7], against density-functional theory calculations gives higher values of ϵ, and smaller absolute values of σ and q. These are included in Table S1 for comparison only.

II. SMALL-ANGLE NEUTRON SCATTERING

A repository for the recreation of the analysis in the main article and in the supporting information is available at doi.org/10.5281/zenodo.7506870.

A. Model details

The theoretical scattering intensity, $I(Q)$, of the 'ellipsoid' model used to fit the SANS data is calculated with the orientational average of the spheroid form factor amplitude, $F(Q,\ u)$ as follows.

$$I(Q) = \frac{C}{V}\left\langle |F(Q)|^2 \right\rangle + B \tag{S1a}$$

$$\left\langle |F(Q)|^2 \right\rangle = \int_0^1 |F(Q,\ u)|^2\, du \tag{S1b}$$

$$F(Q,\ u) = \Delta\beta V \frac{3\left(\sin QR - QR\cos QR\right)}{(QR)^3} \tag{S1c}$$

$$R = R_{\mathrm{e}}\left[1 + u^2\left(\frac{R_{\mathrm{p}}^2}{R_{\mathrm{e}}^2} - 1\right)\right]^{1/2} \tag{S1d}$$

Here, B and C are the background and scale factor parameters respectively, and $\Delta\beta$ is the difference in scattering length density, β, between the scattering spheroid and the solvent. R_{e} and R_{p} are the equatorial and polar radii of the spheroid, and the volume of spheroid is defined as $V = R_{\mathrm{p}}R_{\mathrm{e}}^2 4\pi/3$.

This model was reparameterised so that V was fit alongside an eccentricity parameter, which was defined as $e = R_{\mathrm{p}}/R_{\mathrm{e}}$. The scattering length density of the spheroid, β_{sph}, was defined as a function of the scattering length densities and volume fractions, ϕ, of GMO, water (w) and solvent (s) as follows.

$$\beta_{\mathrm{sph}} = \beta_{\mathrm{GMO}}\phi_{\mathrm{GMO}} + \beta_{\mathrm{w}}\phi_{\mathrm{w}} + \beta_{\mathrm{s}}\phi_{\mathrm{s}} \tag{S2a}$$

$$\phi_{\mathrm{GMO}} = 1 - \frac{V\phi_{\mathrm{s}} + V_{\mathrm{w}}}{V} \tag{S2b}$$

$$V_{\mathrm{w}} = \frac{\upsilon\left[V - (V\phi_{\mathrm{s}})\right]}{\upsilon + 1} \tag{S2c}$$

$$\upsilon = \omega\frac{N_{\mathrm{GMO}}}{N_{\mathrm{w}}} \tag{S2d}$$

Here, ω is the hydration ratio while N_{GMO} and N_{w} are, respectively, the number densities of GMO and water. In all cases, the volume fraction of the solvent was fixed at 0 due to

perfect correlation with the scale factor parameters. The parameters and their respective priors for the dry and wet systems are shown in Tables S2 and S3.

TABLE S2. Parameters and their priors used to model the SANS data collected with the GMO-dodecane solution.

Parameter	Initial value	Prior range
V / Å^3	13000	$(0,\ 10^8)$
e	1.88	$(0.333,\ 3)$
C	0.0033	$(10^{-6},\ 1)$
B / cm^{-1}	0.00975	$(10^{-3},\ 1)$
β_{GMO} / Å$^{-2} \times 10^{-6}$	0.21	–
β_{w} / Å$^{-2} \times 10^{-6}$	0	–
ω	0	–
ϕ_{s}	0	–

TABLE S3. Parameters and their priors used to model the SANS data collected with the GMO-water-dodecane solutions. Values for D_2O^* and $H_2O^\dagger$.

Parameter	Initial value	Prior range
V / Å^3	13000	$(0,\ 10^8)$
e	1.88	$(0.333,\ 3)$
C_{D_2O}	0.01	$(10^{-6},\ 1)$
C_{H_2O}	0.01	$(10^{-6},\ 1)$
B_{D_2O} / cm^{-1}	0.00975	$(10^{-3},\ 1)$
B_{H_2O} / cm^{-1}	0.00975	$(10^{-3},\ 1)$
β_{GMO} / Å$^{-2} \times 10^{-6}$	0.21	–
β_w / Å$^{-2} \times 10^{-6}$	6.37^* / $-0.54^\dagger$	–
ω	5	–
ϕ_s	0	–

B. Results

The parameter values for the dry and wet systems are shown in Tables S4 and S5. The parameter distributions and correlations are visualised in Fig. S1 and Fig. S2 for the dry and wet system respectively.

TABLE S4. The mode centres and the 95 % highest density intervals (HDIs) of the posterior distributions of the parameters. This statistic was used to describe the parameter distributions due to bimodal characteristics. The two modes of e are described by two intervals as the modes are discrete. However, the two modes for C and V are encapsulated by one 95 % HDI interval. The centres of the modes are estimated by taking the mean of the 1 % HDI of each mode.

V / Å$^3 \times 10^4$	e		$C \times 10^3$	B / cm$^{-1} \times 10^{-2}$
$3.11^{+0.28}_{-0.14}$	$0.48^{+0.07}_{-0.06}$,	$1.88^{+0.12}_{-0.13}$	$3.56^{+0.16}_{-0.29}$	$1.08^{+0.17}_{-0.13}$

TABLE S5. The median and 95 % credible intervals for each parameter used to fit the SANS data collected with the GMO-water-dodecane solutions.

V / Å$^3 \times 10^5$	e	$C_{H_2O} \times 10^2$	B_{H_2O} / cm$^{-1} \times 10^{-2}$	B_{D_2O} / cm$^{-1} \times 10^{-2}$	$C_{D_2O} \times 10^2$
$1.26_{\mathcal{N}} \pm 0.01$	0.66 ± 0.01	0.61 ± 0.00	$0.89_{\mathcal{N}} \pm 0.09$	$1.62_{\mathcal{N}} \pm 0.08$	0.52 ± 0.00

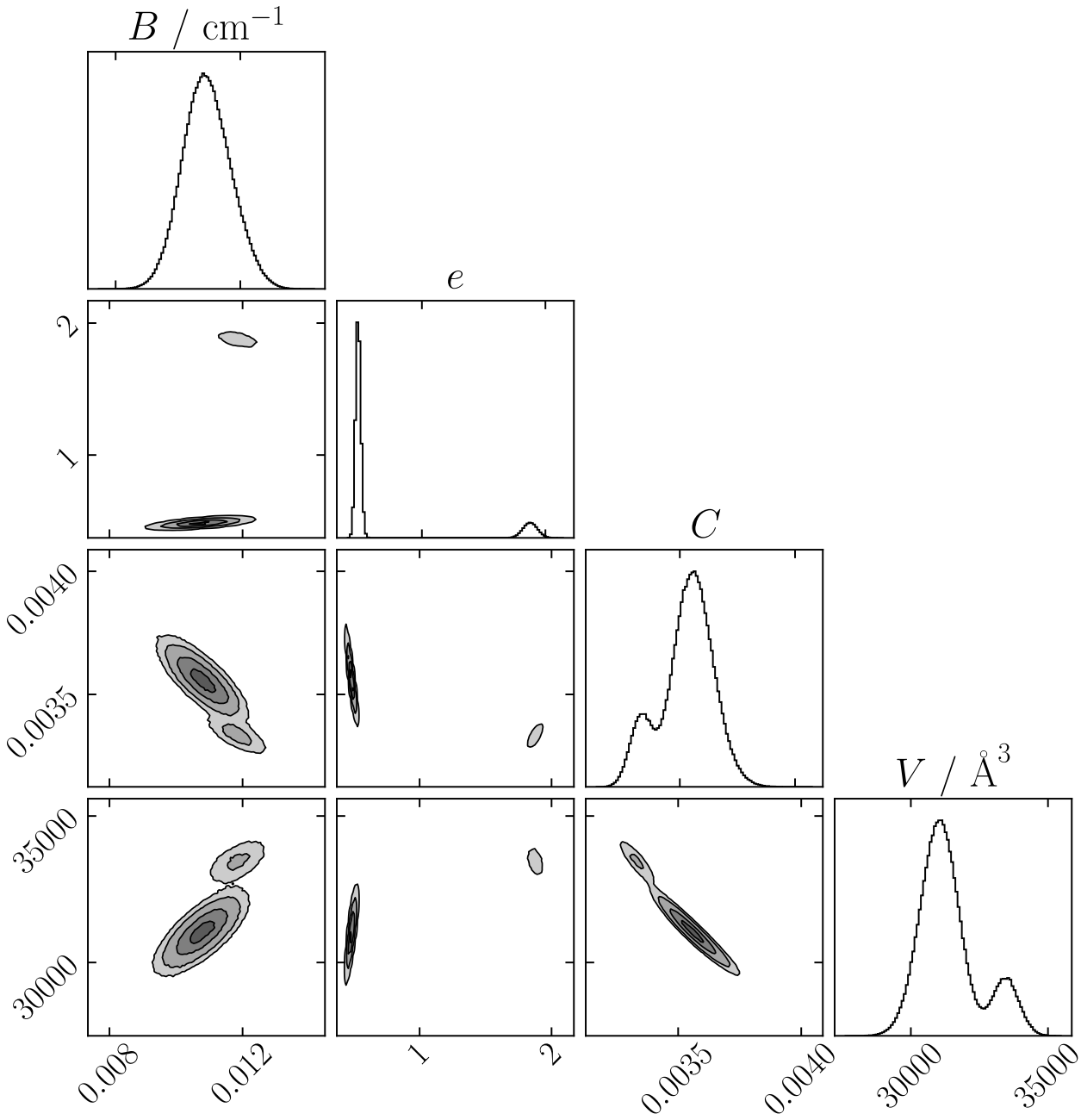

FIG. S1. Corner plot of the posterior distribution of the parameters used to fit the SANS data of the dry GMO system.

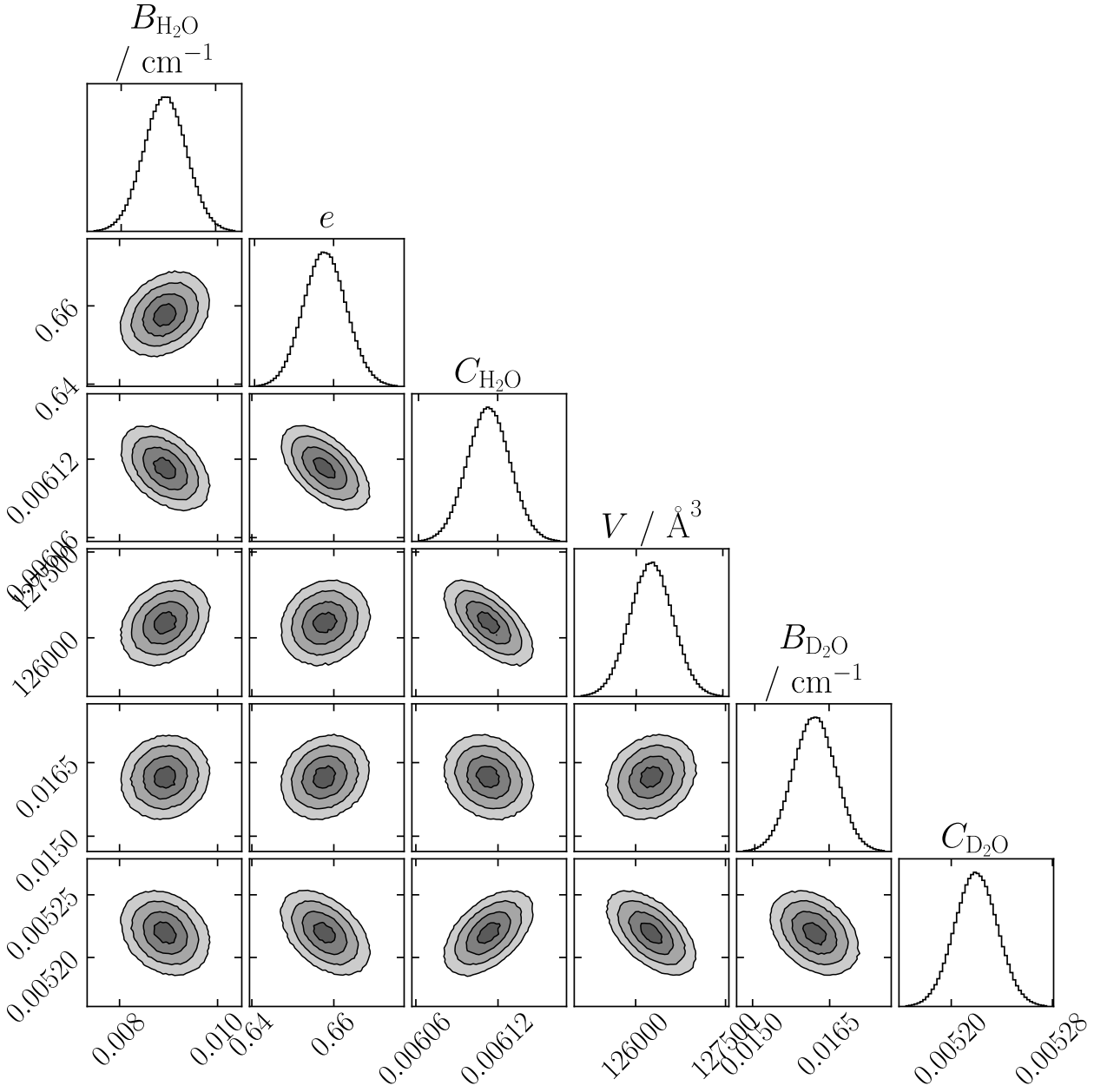

FIG. S2. Corner plot of the posterior distribution of the parameters used to fit the SANS data of the wet GMO system.

III. NEUTRON REFLECTOMETRY: NEAT *N*-DODECANE

A. Model details

The adventitious layer was modelled with a nuclear scattering length density β_{nuc}, a thickness d, a Gaussian RMS roughness σ, and a solvation ϕ_{s} defined as the volume fraction of solvent within the layer. The scattering length density of the solvated layer is then a combination of the solvent scattering length density, β_{s}, and the scattering length density of the adsorbate, β_{ads}, weighted by the respective volume fractions:

$$\beta_{\mathrm{nuc}} = \phi_{\mathrm{s}}\beta_{\mathrm{s}} + (1 - \phi_{\mathrm{s}})\,\beta_{\mathrm{ads}}. \tag{S3}$$

In addition, the magnetic scattering length density, β_{mag}, of iron was parameterised using

$$\beta_{\mathrm{mag}} = \frac{C\mu\beta_{\mathrm{nuc}}}{b_{\mathrm{Fe}}}, \tag{S4}$$

where μ is the fitted magnetic moment of iron in Bohr magnetons, $C = 2.699 \times 10^{-5}$ Å μ_{B}^{-1} (see Section III A 1), and $b_{\mathrm{Fe}} = 9.45$ fm is the scattering length of iron [9]. This approach was not used for the iron oxide magnetic scattering length density, because the precise phase of the iron oxide is unknown.

1. Derivation of constant C in eqn (S4)

The magnetic scattering length density for a magnetic thin film can be defined as

$$\beta_{\mathrm{mag}} = \frac{-m_{\mathrm{n}}}{2\pi\hbar^2}\boldsymbol{\mu}_{\mathrm{m}} \cdot \boldsymbol{B} \tag{S5}$$

where m_{n} is the mass of a neutron, $\boldsymbol{\mu}_{\mathrm{m}}$ is the magnetic moment of a neutron, and $\boldsymbol{B}$ is the magnetic flux density [10]. Using CODATA [11] physical constants as shown in Table S6, eqn (S5) can be written as

$$\beta_{\mathrm{mag}} = C'\boldsymbol{\mu}_{\mathrm{m}} \cdot \boldsymbol{B} \tag{S6}$$

where $C' = -2.397 \times 10^{40}$ m^{-2} J^{-1}. In specular neutron reflectometry, only the in-plane component of a layer's magnetisation, $\boldsymbol{M}_{\parallel}$, contributes to the reflected intensity [12]. Therefore, β_{m} can be defined as

$$\beta_{\mathrm{mag}} = C'\mu_0\boldsymbol{\mu}_{\mathrm{m}} \cdot \boldsymbol{M}_{\parallel} = C''\boldsymbol{\mu}_{\mathrm{m}} \cdot \boldsymbol{M}_{\parallel} \tag{S7}$$

where μ_0 is the permeability of free space and $C'' = -3.012 \times 10^{34}$ m^{-3} A^{-2}. The in-plane component of a material's magnetic moment, $\boldsymbol{\mu}_{\parallel}$, in Bohr magnetons is related to the in-plane component of the magnetisation: $\boldsymbol{M}_{\parallel} = \boldsymbol{\mu}_{\parallel} N \mu_{\mathrm{B}}$, where N is the number density of the material and μ_{B} is the Bohr magneton. Due to the parallel or antiparallel orientation of the neutron spin with respect to a domain's magnetisation, $\boldsymbol{\mu}_{\mathrm{m}} \cdot \boldsymbol{M}_{\parallel} = |\boldsymbol{\mu}_{\mathrm{m}}| \times |\boldsymbol{\mu}_{\parallel}| N \mu_{\mathrm{B}}$. As such, $C = C'' \times \mu_{\mathrm{B}} \times |\boldsymbol{\mu}_{\mathrm{m}}| = 2.699 \times 10^{-5}$ Å μ_{B}^{-1}.

TABLE S6. The physical constants and their values used in the derivation of C.

m_{n} / kg	$\lvert\boldsymbol{\mu}_{\mathrm{m}}\rvert$ / J T^{-1}	μ_0 / kg m s^{-2} A^{-2}	μ_{B} / A m^2
1.6749×10^{-27}	-9.6624×10^{-27}	1.2566×10^{-6}	9.2740×10^{-24}

2. Parameters and priors

The parameters, and their uniform priors, of the model to describe the NR data collected with neat dodecane are described in Table S7.

TABLE S7. The initial values and the prior bounds used when modelling the NR data collected with neat dodecane. The superscript and subscript values are the upper and lower bounds of the prior uniform distributions. Those values without lower and upper bounds were held constant throughout the fit. The priors and initial values of the underlying substrate and solvent were kept the same when modelling the data without the adventitious layer (AL).

Layer	β_{nuc} / 10^{-6} Å^{-2}	β_{mag} / 10^{-6} Å^{-2}	μ / μ_{B}	d / Å	σ / Å	ϕ / %
Si	2.07	–	–	∞	3	–
SiO_2	3.47	–	–	15^{25}_{1}	4^{10}_{1}	–
Fe	$8.02^{8.10}_{7.50}$	–	$2.1^{2.2}_{1.9}$	190^{210}_{170}	5^{15}_{1}	–
FeO_x	$7.00^{7.20}_{5.00}$	$0.5^{1.30}_{0.00}$	–	30^{40}_{20}	6^{15}_{1}	–
AL	$0.00^{6.00}_{-0.54}$	–	–	10^{20}_{1}	7^{15}_{1}	0^{100}_{0}
dod-d_{26}	$6.70^{6.70}_{5.00}$	–	–	–	–	–
dod-h_{26}	-0.46	–	–	–	–	–

B. Results

The parameter posterior values from the fit to the NR data collected with neat dodecane are given in Table S8.

TABLE S8. Median and 95% credible interval values for the parameters of each layer used to model the NR from the neat dodecane system. The minimum number of independent samples was estimated to be 56091.

Layer	β_{nuc} / 10^{-6} Å^{-2}	β_{mag} / 10^{-6} Å^{-2}	μ / μ_{B}	d / Å	σ / Å	ϕ / %
Si	2.07	–	–	∞	3	–
SiO_2	3.47	–	–	$19.5^{+1.5}_{-1.7}$	$6.1^{+1.0}_{-1.2}$	–
Fe	$7.88_{\mathcal{N}} \pm 0.07$	–	$2.11_{\mathcal{N}} \pm 0.04$	$189.9^{+0.7}_{-0.9}$	$11.3^{+0.9}_{-1.2}$	–
FeO_x	$5.71^{+0.2}_{-0.1}$	$0.10^{+0.17}_{-0.09}$	–	$32.8^{+1.3}_{-1.1}$	$3.1^{+2.4}_{-2.0}$	–
AL	$0.22^{+0.57}_{-0.72}$	–	–	13.7 ± 2.1	$2.5^{+2.7}_{-1.5}$	$18.1^{+9.2}_{-15.2}$
dod-d_{26}	$6.20^{+0.04}_{-0.05}$	–	–	–	–	–
dod-h_{26}	-0.46	–	–	–	–	–

IV. NEUTRON REFLECTOMETRY: GMO IN *N*-DODECANE

A. Model details

TABLE S9. Priors used for modelling the GMO layer across the three different candidate models. All prior distributions were uniform. The final column shows the natural logarithm of the Bayesian evidence for the three models.

Model	β_{nuc} / 10^{-6}Å^{-2}	d / Å	σ / Å	ϕ / %	$\ln Z$
1	0.21	20^{30}_{10}	1^{15}_{1}	0^{100}_{0}	1184.1 ± 0.3
2	$0.21^{6.00}_{-0.54}$	20^{30}_{10}	1^{15}_{1}	0	1182.4 ± 0.5
3	$0.21^{6.00}_{-0.54}$	20^{30}_{10}	1^{15}_{1}	0^{100}_{0}	1179.0 ± 0.5

B. Results

The parameter posterior values from the fit to the NR data collected with neat dodecane are given in Table S10. The nuclear and magnetic scattering length density profiles of the dodecane-d_{26} contrast is given in Fig. S3. The corner plot in Fig. S4 shows the posterior distributions of the parameters.

TABLE S10. Median and 95% credible interval values for the parameters of each layer in the GMO-dodecane system. The minimum number of independent samples was estimated to be 44646.

Layer	β_{nuc} / 10^{-6} Å^{-2}	β_{mag} / 10^{-6} Å^{-2}	μ / μ_{B}	d / Å	σ / Å	ϕ / %
Si	2.07	–	–	∞	3	–
SiO_2	3.47	–	–	18.3 ± 1.3	$9.9^{+0.2}_{-0.3}$	–
Fe	7.91 ± 0.06	–	$2.09_{\mathcal{N}} \pm 0.04$	$189.7^{+0.7}_{-0.8}$	$11.9^{+0.8}_{-0.9}$	–
FeO_x	$5.64^{+0.17}_{-0.14}$	$0.11^{+0.17}_{-0.11}$	–	34.5 ± 0.4	$4.8^{+2.2}_{-2.4}$	–
GMO	0.21	–	–	$19.4^{+1.8}_{-1.6}$	$6.0^{+1.6}_{-2.1}$	8.6 ± 8.1
dod-d_{26}	$6.32^{+0.04}_{-0.02}$	–	–	–	–	–
CMdod	1.93 ± 0.01	–	–	–	–	–
dod-h_{26}	-0.46	–	–	–	–	–

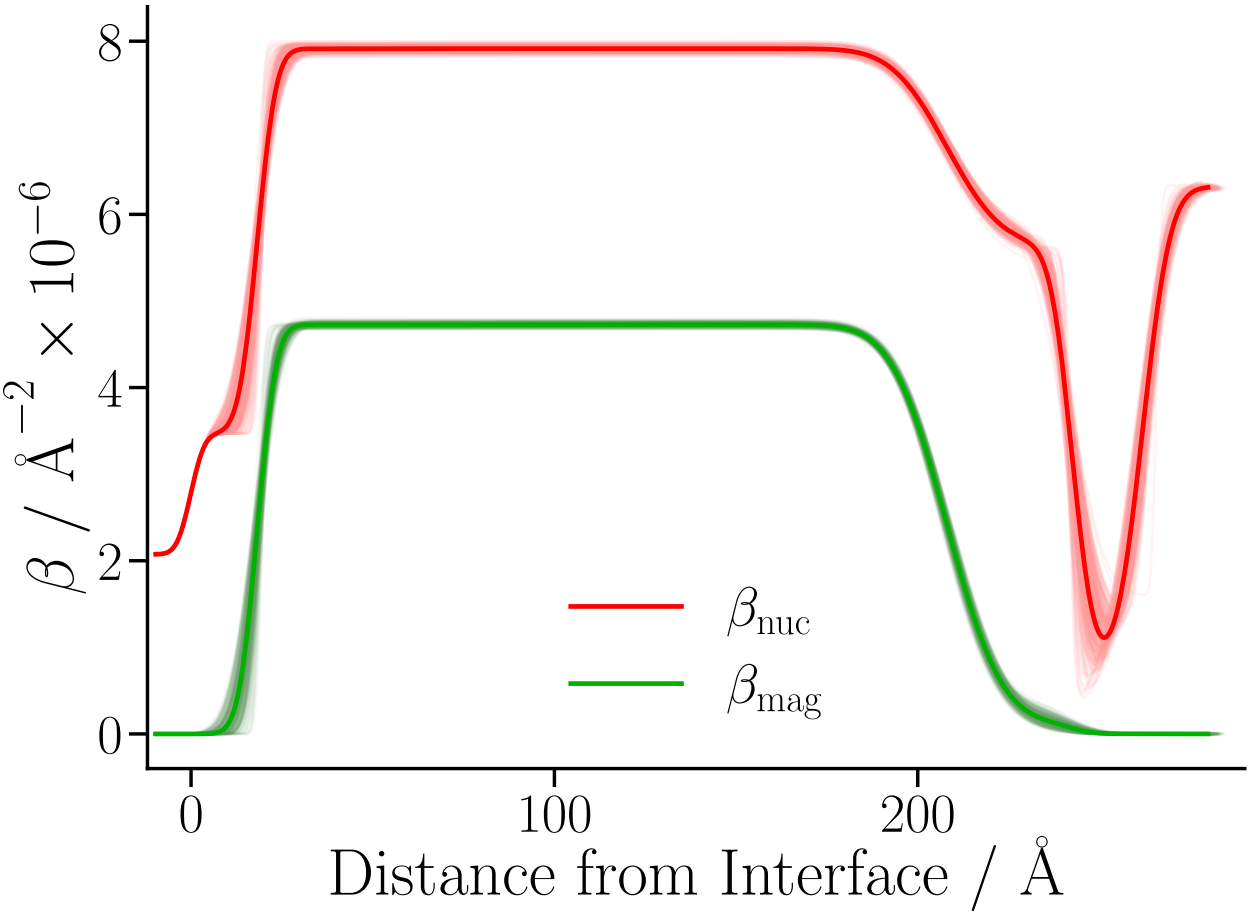

FIG. S3. Magnetic scattering length density, β_{mag}, and nuclear scattering length density profile of the GMO-dodecane system. The β_{nuc} profile shown is the dodecane-d_{26} contrast.

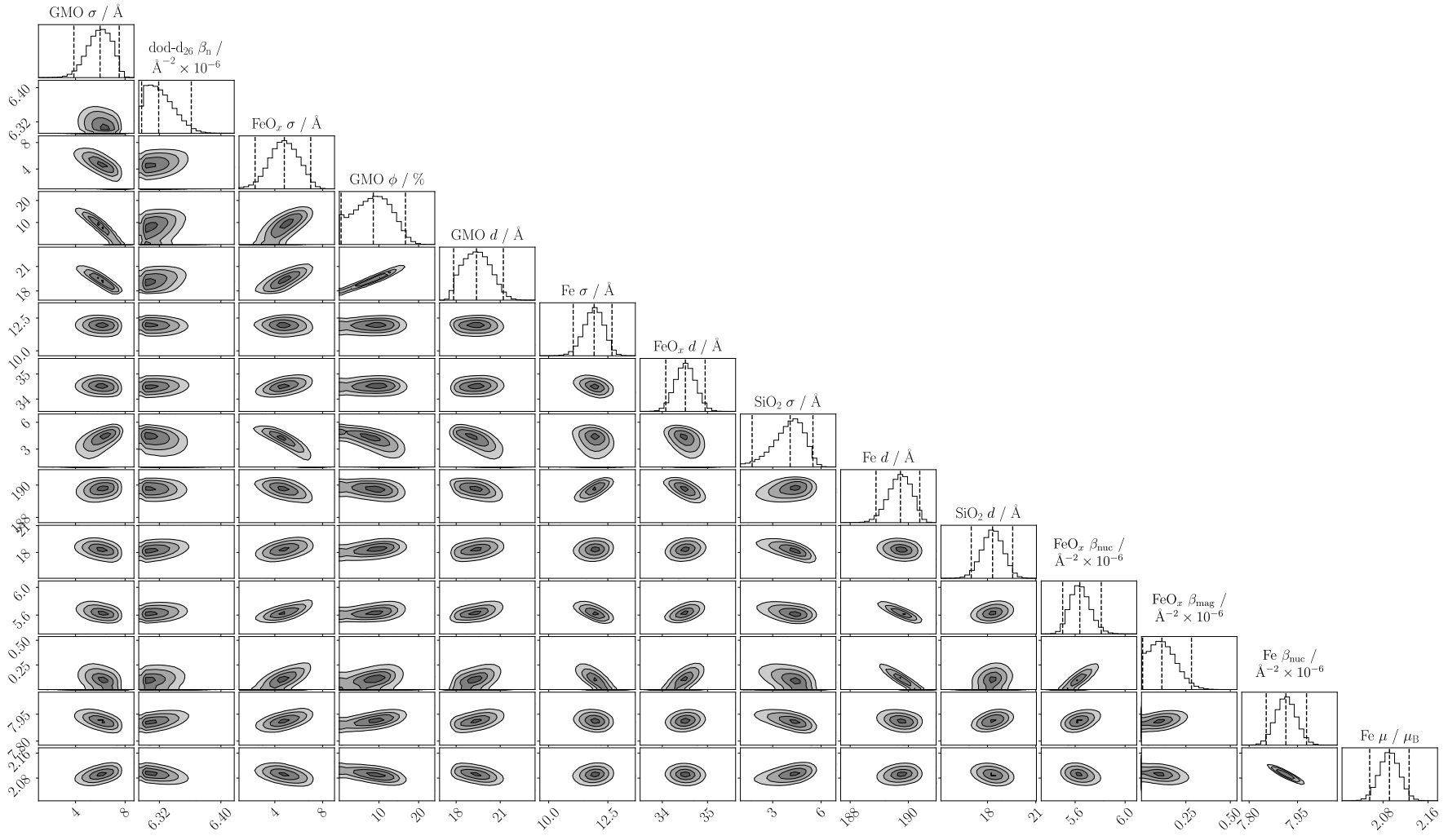

FIG. S4. Corner plot of the posterior distribution of the parameters used to fit the data collected with GMO in dodecane without added water.

V. NEUTRON REFLECTOMETRY: GMO IN *N*-DODECANE WITH ADDED WATER

A. Model details

As described in the main article, two models were proposed to describe the reflectivity collected with the GMO solutions doped with water. These are referred to as the single-layer (SL) model and the double-layer (DL) model. In the SL model, the interfacial layer is modelled as a homogeneus mixture of GMO, water (w), and solvent (s), and so the combined nuclear scattering length density of the layer is

$$\beta_{\mathrm{nuc}} = \beta_{\mathrm{s}}\phi_{\mathrm{s}} + \beta_{\mathrm{GMO}}\phi_{\mathrm{GMO}} + \beta_{\mathrm{w}}\left(1 - \phi_{\mathrm{s}} - \phi_{\mathrm{GMO}}\right) \tag{S8}$$

where β and ϕ are the nuclear scattering length densities and volume fractions of the species.

The DL model was defined in a similar manner. The first interfacial layer adjacent to the iron oxide surface, referred to as the 'inner' layer, was assumed to contain GMO head groups, water, and solvent. As such, the scattering length density of the inner layer was modelled using eqn (S8), but with β_{GMO} and ϕ_{GMO} replaced by β_{head} and ϕ_{head}, respectively. The upper bound of the inner-layer thickness was restricted to 6.6 Å, representing the approximate extended length of the GMO head group. As the density of the GMO head groups cannot be assumed to be the same as the average density of GMO molecules, β_{head} was treated as a fit parameter.

The second interfacial layer, referred to as the 'outer' layer, was parameterised so that the surface excess of the GMO tail groups was equal to that of the GMO head groups in the inner layer. This will be expanded upon later. Additionally, the scattering length density of the tail, β_{tail}, was constrained so that

$$\beta_{\mathrm{tail}} = \frac{b_{\mathrm{tail}}}{\left(\overline{V}_{\mathrm{GMO}} - \overline{V}_{\mathrm{head}}\right)} \tag{S9}$$

where $b_{\mathrm{tail}} = -10.4$ fm is the scattering length of the GMO tail group [9]. $\overline{V}_{\mathrm{head}}$ is the average volume of the GMO head group, given by $b_{\mathrm{head}}/\beta_{\mathrm{head}}$, where $b_{\mathrm{head}} = 23.6$ fm is the scattering length of the head group [9]. Similarly, $\overline{V}_{\mathrm{GMO}} = b_{\mathrm{GMO}}/\beta_{\mathrm{GMO}} = 1/N_{\mathrm{GMO}}$ is the average volume of a GMO molecule given by the reciprocal of the GMO number density. This constraint relies upon $\overline{V}_{\mathrm{GMO}} = \overline{V}_{\mathrm{head}} + \overline{V}_{\mathrm{tail}}$, where $\overline{V}_{\mathrm{tail}}$ is the average volume of the

tail group. The volume fractions of water and solvent within the outer layer were defined in a similar manner to the inner layer. However, a volume fraction of physisorbed GMO was also included in the outer layer, which was modelled with the nominal scattering length density for GMO. Therefore, this model is an extension of the SL system, but one which allows for an inhomogeneous composition of the interface with respect to GMO, water, and solvent.

Initial fits to the data suggested that the iron oxide roughness was larger than the upper bound of the inner layer thickness. Layers with thicknesses less than the roughnesses of adjacent films can lead to models with non-physical characteristics, and in particular, negative volume fractions. When using a typical slab model with the Névot-Croce factor, the volume fraction profile of the m^{th} layer, $\Phi_m(z)$, in a series of M layers $(1,\ 2,\ 3, \cdots M)$ is calculated as the difference of the cumulative distribution functions, $F(z)$, of the $(m-1)^{\text{th}}$ and m^{th} interfaces:

$$\Phi_m(z) = F_{m-1}(z) - F_m(z), \tag{S10}$$

where $F_0(z) = 1$ and $F_M(z) = 0$. In this framework, each $F_m(z)$ is defined by the thickness of the m^{th} layer and the Gaussian roughness of $(m+1)^{\text{th}}$ layer. Therefore, negative volume fractions arise when $F_m(z) > F_{m-1}(z)$, which can occur with thin films that are bounded by interfaces of differing widths. Note that the fronting and backing mediums are treated as the first and final (1^{st} and M^{th}) layers respectively in this framework. The occurrence of negative volume fractions was avoided by redefining the volume fraction profile of each layer as follows.

$$\Phi_{\text{Si}}(z) = [1 - F_1(z)]\,[1 - F_2(z)] \tag{S11a}$$

$$\Phi_{\text{SiO}_2}(z) = F_1(z)\,[1 - F_2(z)] \tag{S11b}$$

$$\Phi_{\text{Fe}}(z) = F_2(z)\,[1 - F_3(z)] \tag{S11c}$$

$$\Phi_{\text{FeO}_x}(z) = F_3(z)\,[1 - F_4(z)] \tag{S11d}$$

$$\Phi_{\text{SL}}(z) = F_3(z)F_4(z)\,[1 - F_5(z)] \tag{S11e}$$

$$\Phi_{\text{inner, DL}}(z) = F_3(z)F_4(z)\,[1 - F_5(z)] \tag{S11f}$$

$$\Phi_{\text{outer, DL}}(z) = F_3(z)F_4(z)F_5(z)\,[1 - F_6(z)] \tag{S11g}$$

$$\Phi_{\text{solvent, SL}}(z) = F_3(z)F_4(z)F_5(z) \tag{S11h}$$

$$\Phi_{\text{solvent, DL}}(z) = F_3(z)F_4(z)F_5(z)F_6(z) \tag{S11i}$$

Due to the thickness of the iron layer, F_2 and F_3 do not overlap and so the curvature of $\Phi_{\mathrm{Fe}}(z)$ was assumed to be strictly Gaussian. In this framework, F_m represent the ratios of the cross-sectional areas of the layers over the z direction, $A_m(z)$, as laid out below for the SL model.

$$F_1(z) = \frac{A_{\mathrm{SiO_2}}(z)}{A_{\mathrm{Si}}(z) + A_{\mathrm{SiO_2}}(z)} \tag{S12a}$$

$$F_2(z) = \frac{A_{\mathrm{Fe}}(z)}{A_{\mathrm{Si}}(z) + A_{\mathrm{SiO_2}}(z) + A_{\mathrm{Fe}}(z)} \tag{S12b}$$

$$F_3(z) = \frac{A_{\mathrm{FeO}_x}(z) + A_{\mathrm{SL}}(z) + A_{\mathrm{s}}(z)}{A_{\mathrm{Si}}(z) + A_{\mathrm{SiO_2}}(z) + A_{\mathrm{Fe}}(z) + A_{\mathrm{FeO}_x}(z) + A_{\mathrm{SL}}(z) + A_{\mathrm{s}}(z)} \tag{S12c}$$

$$F_4(z) = \frac{A_{\mathrm{SL}}(z) + A_{\mathrm{s}}(z)}{A_{\mathrm{FeO}_x}(z) + A_{\mathrm{SL}}(z) + A_{\mathrm{s}}(z)} \tag{S12d}$$

$$F_5(z) = \frac{A_{\mathrm{s}}(z)}{A_{\mathrm{SL}}(z) + A_{\mathrm{s}}(z)} \tag{S12e}$$

Note that F_4 and F_5 must be redefined for the DL system.

This model assumes the asperities of the Fe layer can penetrate through the SiO_2 layer into the Si at some points across the horizontal plane, along with penetrating through the iron oxide into the adsorbed layer. In other words, the model allows for a proportion of the interfacial area of the Si and Fe layers where they are not bound by their analogous oxide layers. The volume fractions of each layer were calculated over the whole interface in steps of approximately 0.5 Å using the thickness and Gaussian roughness parameters that were fit. Then, the scattering length density over the interface for each contrast, $\beta(z)$, was calculated following eqn (S13):

$$\beta(z) = \sum_{m=1}^{M} \Phi_m(z)\, \beta_m \tag{S13}$$

where β_m is the scattering length density of the m^{th} layer given by

$$\beta_m = \sum_i \phi_i \left(\beta_{i,\,\mathrm{nuc}} \pm \beta_{i,\,\mathrm{mag}}\right) \tag{S14}$$

for the up-spin (+) and down-spin (−) states respectively. Here, ϕ_i is the volume fraction of the i^{th} component within a layer. Micro-slabs of ~ 0.5 Å were then modelled with $\beta(z)$; the roughness of each interface between the micro-slabs was zero and was represented by Heaviside step functions. Where the volume fraction of a layer was non-zero but differed less than 1×10^{-5}, the volume fraction was estimated to be constant and the thickness of this

region was extended to the point at which the volume fraction began to deviate more than this limit. This minimised the number of micro-slabs modelled in the Abelès formalism.

The surface excess of the i^{th} component within the m^{th} layer can be calculated following eqn (15Adsorption onto iron oxide surfaces: neutron reflectometry of GMO in dodecaneequation.3.15), assuming that the integral of $\Phi_m(z)$ is equal to the distance d between the bounding interfaces of the m^{th} layer. In general, this is true for models calculated using eqn (S10). However, in this case, the integrals of the volume fraction profiles for the inner and outer layers are poorly estimated by their thicknesses. Therefore, the surface excess of the GMO head groups within the inner layer was calculated using

$$\Gamma_{\text{heads}} = \frac{\beta_{\text{heads}}}{b_{\text{heads}}} \phi_{\text{heads}} \left(1 - \phi_{\text{s, inner}}\right) \int \Phi_{\text{inner}}(z)\, dz \tag{S15}$$

where $\phi_{\text{s, inner}}$ is the volume fraction of solvent within the inner layer. As the surface excess of GMO tail groups within the outer layer is constrained to be equal to the GMO head groups within the inner layer, the volume fraction of GMO tail groups, ϕ_{tails}, within the outer layer is

$$\phi_{\text{tails}} = \Gamma_{\text{heads}} \frac{b_{\text{tails}}}{\beta_{\text{tails}}} \frac{1}{\int \Phi_{\text{outer}}(z)\, dz}\,. \tag{S16}$$

The models were also run with inequality constraints so that the only considered solutions were those where the thicknesses of the SL, inner, outer and SiO_2 layers were at least twice their roughnesses. This was done so that 95 % of the negative vertical deviations from the m^{th} interface fell within the thickness of the m^{th} layer, ensuring that only slab-like layers were considered to describe these thin films.

TABLE S11. The initial values and uniform priors of the parameters used to fit the NR data collected with the GMO-dodecane solutions doped with water. *Two dodecane-d_{26} layers were modelled to account for the differences in β_n with either H_2O or D_2O doped within the solvent. †The priors for the parameters of the physisorbed GMO.

Layer	β_{nuc} / 10^{-6} Å^{-2}	β_{mag} / 10^{-6}Å^{-2}	μ / μ_B	d / Å	σ / Å	ϕ_{GMO} / %	ϕ_s / %
Si	2.07	–	–	∞	3	–	–
SiO_2	3.47	–	–	15^{25}_{1}	4^{15}_{1}	–	–
Fe	$8.02^{8.10}_{7.50}$	–	$2.1^{2.2}_{1.5}$	190^{230}_{190}	5^{20}_{1}	–	–
FeO_x	$7.00^{7.20}_{5.00}$	$0.5^{1.30}_{0.00}$	–	30^{60}_{20}	1^{15}_{1}	–	–
dod-d_{26}*	$6.70^{6.70}_{5.00}$	–	–	–	–	–	–
dod-h_{26}	-0.46	–	–	–	–	–	–
SL	0.21	–	–	25^{40}_{10}	7^{15}_{1}	0^{100}_{0}	0^{100}_{0}
inner DL	1^{2}_{0}	–	–	$5^{6.6}_{1}$	$1^{6.6}_{1}$	0^{100}_{0}	0^{100}_{0}
outer DL	0.21†	–	–	10^{25}_{1}	1^{10}_{1}	0^{100}_{0}†	0^{100}_{0}

B. Results

The parameter values resulting from the fit are shown in Table S12, while the nuclear and magnetic scattering length density profiles of the dodecane-d_{26} contrast which contained D_2O are shown in Fig. S5. Fig. S6 shows the corner plot of the posterior distribution.

The volume fraction profiles of each i^{th} component in the model are shown in Fig. 10NR data collected with the dodecane samples stirred with D_2O and the GMO-dodecane-water samples. The darker lines represent the profiles using the median values of the parameter distributions, while the shaded bands are comprised of 300 random samples from the posterior distribution. The data shown in parts (a) and (b) are scaled by a factor of Q^4 to aid comparison. The legend under part (c) describes the colours used in parts (a)–(c), while the legend under (d) refers to (d) only. (a) Comparison of NR data collected with the GMO-dodecane-water solutions to the data of the dodecane samples that were stirred with D_2O. The contrasts collected with dodecane-h_{26} are scaled by 0.1 in the modified reflectivity axis. (b) The fit of the DL model to the data collected with the GMO-dodecane-water solutions. Fitting was conducted with the PT-MCMC sampler implemented in refnx using 10 temperatures. The dodecane-d_{26} contrast collected with H_2O is scaled by 0.1 and the contrast collected with dodecane-h_{26} is scaled by 0.01 in the modified reflectivity axis. (c) The β_{nuc} profiles of the dodecane-d_{26} contrasts. (d) Volume fraction profiles for each component in the DL model.figure.caption.13(d) in the main article. The volume fraction profile of GMO and water were calculated following

$$\begin{aligned}\Phi_i\left(z\right) = \Phi_{\text{inner, DL}}\left(z\right)\phi_{i,\text{ inner}} \\ + \Phi_{\text{outer, DL}}\left(z\right)\phi_{i,\text{ outer}}\,.\end{aligned} \tag{S17}$$

The cross-sectional area, $A_{\text{Si/Fe}}$ where Si was immediately bound by Fe was approximated to be 2.7 % of the total interfacial area of Si through

$$A_{\text{Si/Fe}} = \int_{-10}^{17} \Phi'_{\text{Fe}}\left(z\right)\left[1 - F_1\left(z\right)\right]dz \tag{S18}$$

where $d\Phi_{\text{Fe}}/dz = \Phi'_{\text{Fe}}$. The integral is evaluated between -10 and 17 as both the Si and Fe volume fractions are both non-zero in this range. Similarly, the interfacial area where Fe was not bound by the iron oxide layer, $A_{\text{Fe/noFeO}_x}$, was approximately 1.9 % of the total interfacial area of Fe following:

$$A_{\text{Fe/noFeO}_x} = \int_{170}^{300} \Phi'_{\text{Fe}}\left(z\right)F_4\left(z\right)dz \tag{S19}$$

TABLE S12. Median and 95 % credible interval values for the layer parameters used to model the NR data from the GMO-water-dodecane system. The minimum number of independent samples was estimated to be 20000. †Volume fraction of physisorbed GMO in the outer layer without accounting for solvent.

Layer	β_{nuc} / 10^{-6} Å^{-2}	β_{mag} / 10^{-6} Å^{-2}	μ / μ_{B}	d / Å	σ / Å	ϕ_{GMO} / %	ϕ_{s} / %
Si	2.07	–	–	∞	3	–	–
SiO_2	3.47	–	–	16.3 ± 0.8	$7.9^{+0.4}_{-0.6}$	–	–
Fe	$7.70_{\mathcal{N}} \pm 0.04$	–	$2.06_{\mathcal{N}} \pm 0.03$	$207.7^{+0.7}_{-0.8}$	$15.2^{+0.8}_{-0.9}$	–	–
FeO_x	$6.13^{+0.10}_{-0.09}$	$0.13^{+0.13}_{-0.11}$	–	37.6 ± 0.7	$9.9^{+1.0}_{-1.1}$	–	–
dod-d_{26}-D_2O	6.44 ± 0.02	–	–	–	–	–	
dod-d_{26}-H_2O	6.42 ± 0.02	–	–	–	–	–	
dod-h_{26}	-0.46	–	–	–	–	–	
inner	$1.09^{+0.39}_{-0.64}$	–	–	$6.2^{+0.4}_{-1.2}$	$2.0^{+1.1}_{-1.0}$	$52.3^{+5.3}_{-6.9}$	$5.4^{+6.7}_{-4.8}$
outer	–	–	–	$17.3^{+1.2}_{-1.8}$	$2.5^{+2.9}_{-1.4}$	$34.5^{+56.6\dagger}_{-33.1}$	$22.9^{+4.0}_{-12.0}$

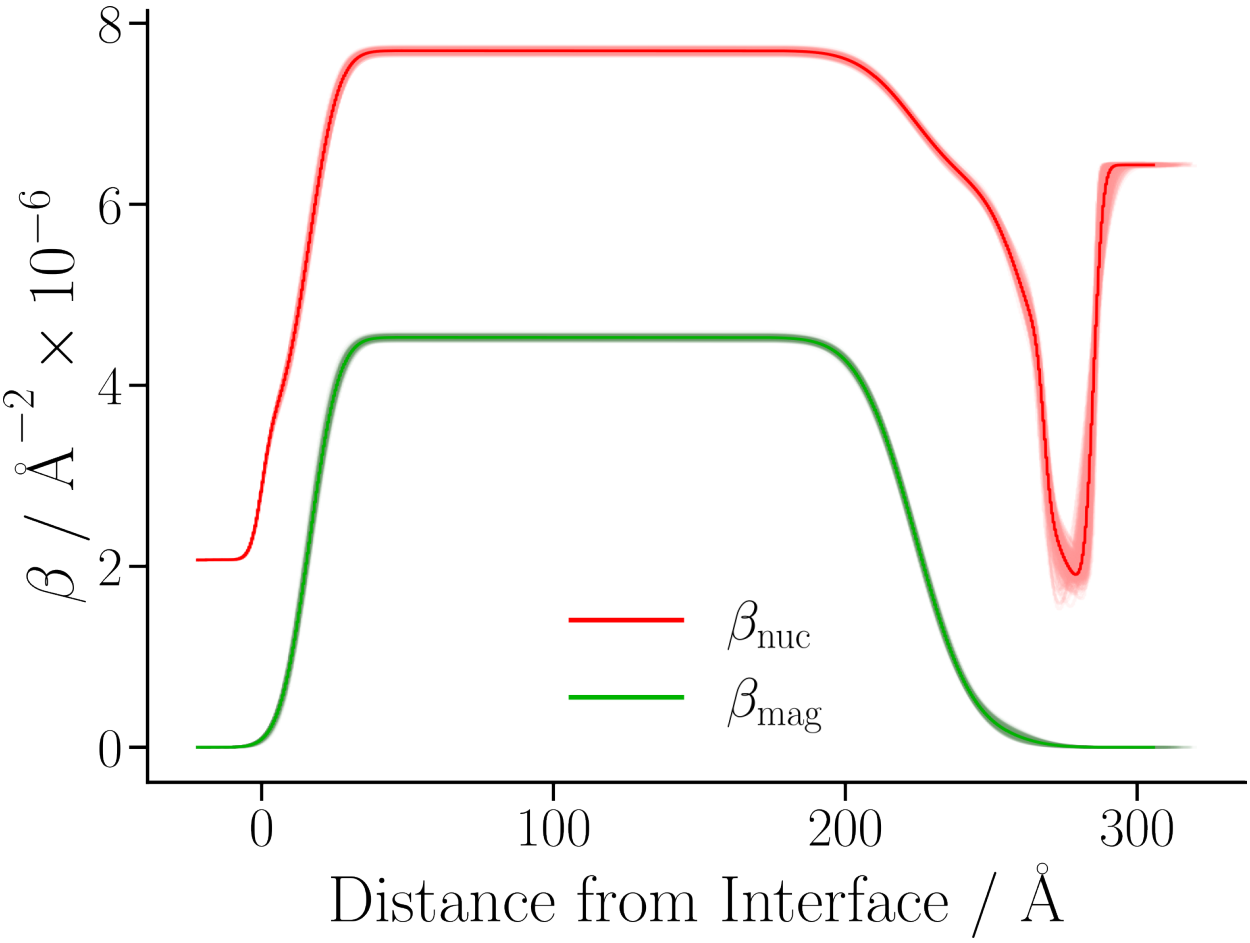

FIG. S5. Magnetic and nuclear scattering length density profiles of the GMO-water-dodecane system. The contrast shown is the dodecane-d_{26} contrast with D_2O.

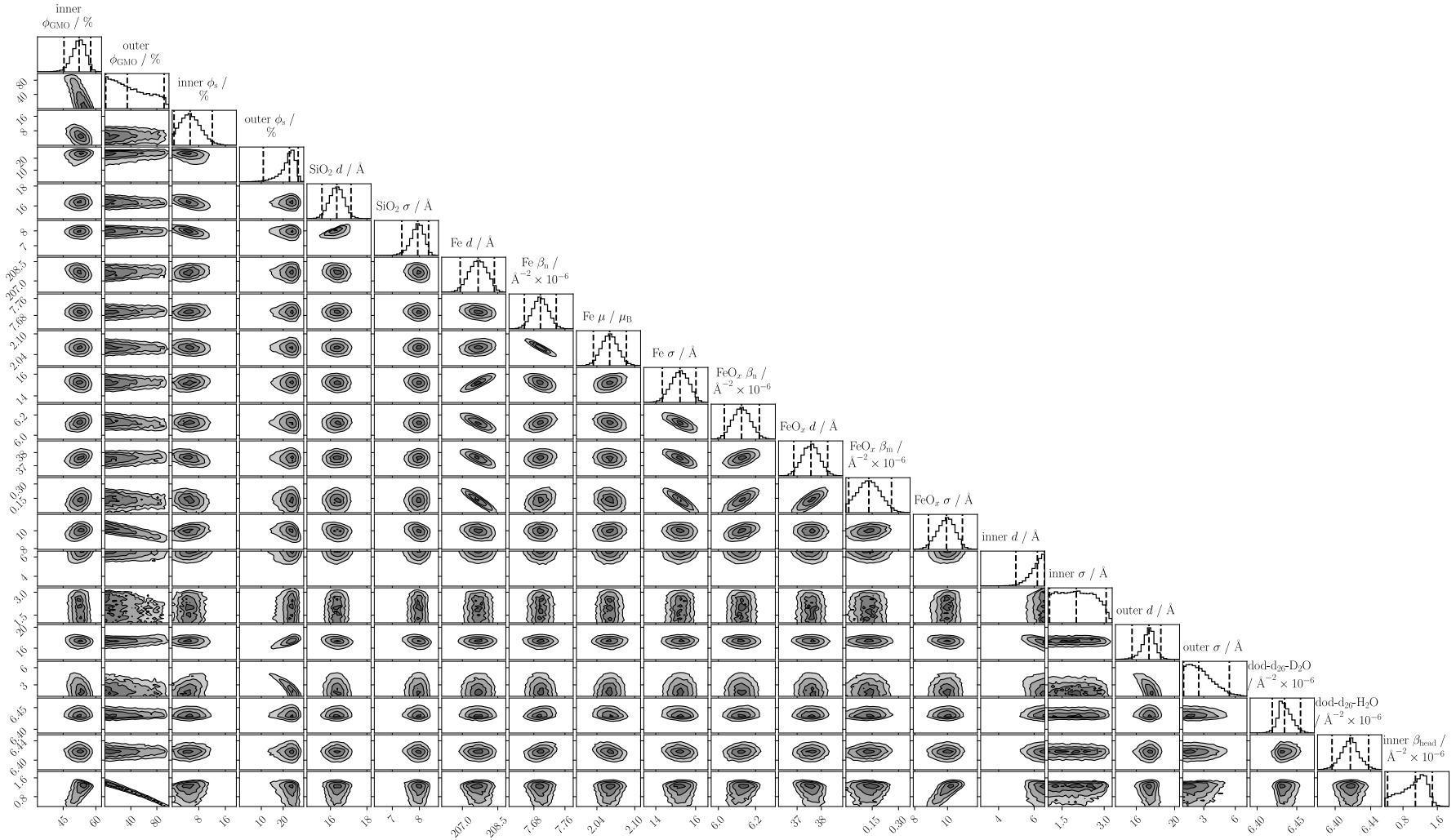

FIG. S6. Corner plot of the posterior distribution of the parameters used to fit the data collected with GMO in dodecane doped with water.

[1] H. Berro, N. Fillot, and P. Vergne, Tribol. Int. **43**, 1811 (2010).

[2] W. L. Jorgensen, J. D. Madura, and C. J. Swenson, J. Am. Chem. Soc. **106**, 6638 (1984).

[3] W. L. Jorgensen and J. Tirado-Rives, J. Am. Chem. Soc. **110**, 1657 (1988).

[4] W. L. Jorgensen, D. S. Maxwell, and J. Tirado-Rives, J. Am. Chem. Soc. **118**, 11225 (1996).

[5] W. Damm, A. Frontera, J. Tirado-Rives, and W. L. Jorgensen, J. Comp. Chem. **18**, 1955 (1997).

[6] M. L. P. Price, D. Ostrovsky, and W. L. Jorgensen, J. Comp. Chem. **22**, 1340 (2001).

[7] S. W. I. Siu, K. Pluhackova, and R. A. Böckmann, J. Chem. Theory Comput. **8**, 1459 (2012).

[8] C. Ayestarán Latorre, J. P. Ewen, C. Gattinoni, and D. Dini, J. Phys. Chem. B **123**, 6870 (2019).

[9] V. F. Sears, Neutron News **3**, 29 (1992).

[10] X. L. Zhou and S. H. Chen, Phys. Rep. **257**, 223 (1995).

[11] NIST Standard Reference Database, `https://physics.nist.gov/cuu/Constants/index.html` (2023), accessed 9 January 2023.

[12] J. Daillant and A. Gibaud, *X-Ray and Neutron Reflectivity: Principles and Applications*, Lecture Notes in Physics, Vol. 770 (Springer, 2008).